

A novel method using machine learning to integrate features from lung and epicardial adipose tissue for detecting the severity of COVID-19 infection

Ni Yao, Ph.D.^{1*}, Yanhui Tian, B.S.^{1*}, Daniel Gama das Neves, MD^{2,3}, Chen Zhao, M.S.⁴, Claudio Tinoco Mesquita, M.D, Ph.D.², Wolney de Andrade Martins, MD, Ph.D.^{3,5}, Alair Augusto Sarmet Moreira Damas dos Santos, MD, Ph.D.^{2,3}, Yanting Li, Ph.D.¹, Chuang Han, Ph.D.¹, Fubao Zhu, Ph.D.¹, Neng Dai, M.D., Ph.D.^{6,7}, Weihua Zhou, Ph.D.^{4,8}

*These authors contributed equally to this work and should be considered co-first authors.

¹School of Computer and Communication Engineering, Zhengzhou University of Light Industry, Zhengzhou, Henan, China

²Department of Radiology, Universidade Federal Fluminense, Rio de Janeiro State, Brazil.

³DASA Complexo Hospitalar de Niterói, Rio de Janeiro State, Brazil

⁴Department of Applied Computing, Michigan Technological University, Houghton, MI, USA

⁵Department of Cardiology, Universidade Federal Fluminense, Rio de Janeiro State, Brazil.

⁶Department of Cardiology, Zhongshan Hospital, Fudan University, Shanghai Institute of Cardiovascular Diseases, Shanghai, China

⁷National Clinical Research Center for Interventional Medicine, Shanghai, China

⁸Center for Biocomputing and Digital Health, Institute of Computing and Cybersystems, and Health Research Institute, Michigan Technological University, Houghton, MI, USA.

Corresponding authors:

Weihua Zhou, PhD

Department of Applied Computing, Michigan Technological University 1400 Townsend Dr, Houghton, MI 49931, USA.

E-Mail: whzhou@mtu.edu

Neng Dai, MD, PhD

Department of Cardiology, Zhongshan Hospital, Fudan University, Shanghai Institute of Cardiovascular Diseases, National Clinical Research Center for Interventional Medicine, 180 Fenglin Road, Xuhui District, Shanghai 200032, China.

E-Mail: niceday1987@hotmail.com

ABSTRACT

Objectives: To investigate the value of radiomics features of epicardial adipose tissue (EAT) combined with lung for detecting the severity of Coronavirus Disease 2019 (COVID-19) infection.

Methods: The retrospective study included data from 515 COVID-19 patients (Cohort1: 415, cohort2: 100) from the two centers between January 2020 and July 2020. A deep learning method was developed to extract the myocardium and visceral pericardium from chest CTs, and then a threshold was applied for automatic EAT extraction. Lung segmentation was achieved according to a published method. Radiomics features of both EAT and lung were extracted for the severity prediction. In a derivation cohort (290, cohort1), univariate analysis and Pearson correlation analysis were used to identify predictors of the severity of COVID-19. A generalized linear regression model for detecting the severity of COVID-19 was built in a derivation cohort and evaluated in internal (125, cohort1) and external (100, cohort2) validation cohorts.

Results: For EAT extraction, the Dice similarity coefficients (DSC) of the two centers were 0.972 (± 0.011) and 0.968 (± 0.005), respectively. For severity detection, the AUC, net reclassification improvement (NRI), and integrated discrimination improvement (IDI) of the model with radiomics features of both lung and EAT increased by 0.09 ($p < 0.001$), 22.4%, and 17.0%, respectively, compared with the model with lung radiomics features, in the internal validation cohort. The AUC, NRI, and IDI increased by 0.04 ($p < 0.001$), 11.1%, and 8.0%, respectively, in the external validation cohort.

Conclusion: Radiomics features of EAT combined with lung have incremental value in detecting the severity of COVID-19.

Keywords: COVID-19 infection; machine learning, chest CT; lung; epicardial adipose tissue

Key Points

A method is proposed to improve the accuracy of epicardial adipose tissue (EAT) extraction.

Both internal (n=125) and external (n=100) validation cohorts demonstrate the incremental value of radiomics features of EAT combined with lung in detecting the severity of COVID-19 infection.

Abbreviations

EAT = epicardial adipose tissue

COVID-19 = coronavirus disease 2019

DSC = Dice similarity coefficients

HD = Hausdorff distance

IDI = integrated discrimination improvement

NRI = net reclassification improvement

Introduction

The COVID-19 pandemic, caused by severe acute respiratory syndrome-coronavirus-2 (SARS-CoV-2), has led to more than 590 million confirmed cases and more than 6.4 million deaths worldwide[1, 2]. Since COVID-19 is a pulmonary infection, primary studies focus on various lung complications. They use lung radiomics features as markers to detect the severity of COVID-19[3-5]. However, due to the lack of consideration of complications, its accuracy is relatively not high.

Inflammation is closely related to the severity of COVID-19 and can provide more value for detecting severity based on lung features[5, 6]. EAT, located between the myocardium and pericardium, is a recognized source of pro-inflammatory mediators[7, 8]. Inflammation affects the progression of COVID-19[9]. Various studies have found an association between EAT volume and the severity of COVID-19, which can help assess the risk of disease progression[10-15].

However, these studies only evaluated EAT volume. With the development of radiomics, more radiomics features of EAT are worthy of inclusion[16, 17]. For the extraction of EAT, traditional methods often require experts to make a tedious and time-consuming annotation. This approach is too slow to exploit its advantages. At the same time, the overall performance of the artificial intelligence method [18, 19] has yet to be improved, so it is necessary and urgent to develop an EAT automatic extraction method with high segmentation accuracy.

In this regard, the aim of the present study is two-fold: (1) to propose an algorithm for EAT automatic extraction; (2) to study the additive value of radiomics features of

both lung and EAT in detecting the severity of COVID-19 infection.

Materials and Methods

Study population

The retrospective study included patients from two centers between January 2020 and July 2020 (**Figure 1**). There were 415 patients (371 mild cases and 44 severe cases) with confirmed COVID-19 cases in Shanghai Public Health Center (Cohort 1) [5] and 100 patients (50 mild and 50 severe) with confirmed COVID-19 cases in Brazil Niteroi Hospital (Cohort 2).

The lung segmentation was achieved according to the research method of Zhao et al.[20], and the segmentation results of lung were confirmed by radiologists. For EAT extraction study, the heart contour of 47 subjects in cohort 1 (27 mild and 20 severe) and 15 subjects in cohort 2 (8 mild and 7 severe) was manually drawn by experienced operators and used to train the segmentation model.

For the classification modeling phase of mild and severe cases, the EAT of the remaining 368 subjects from cohort 1 and 85 subjects from cohort 2 was extracted automatically using a trained deep learning model (Figure 2). 415 patients (371 mild cases and 44 severe cases) with confirmed COVID-19 from cohort 1 were randomly divided into a derivation cohort (n=290, 260 mild cases, 30 severe cases) and an internal validation cohort (n=125, 111 mild cases, 14 cases) (Figure 1). Each case contained its clinical information and a set of chest computed tomography (CT) images in cohort 1. 100 patients (50 mild and 50 severe) from cohort 2 were deemed as an external validation cohort (Figure 1). Each case contains a set of chest CT images in cohort 2.

This study was approved by the Ethics Committee of the Shanghai Public Health Clinical Center and the Brazil Public Health Clinical Center Ethics Committee.

Clinical data collection

For mild-severe classification criteria, in cohort 1, patients with fever, respiratory symptoms, and imaging manifestations of pneumonia were defined as mild patients. Patients with significant lesion progression greater than 50% within 24-48 hours were defined as severe. In cohort 2, patients admitted to the ICU and infirmary were diagnosed with severe COVID-19, and patients who only required treatment in the emergency department were diagnosed with mild COVID-19.

Chest CT procedures

CT scans were performed using Toshiba Aquilion 64 CT scanner in cohort 1. Image acquisition parameters consisted of 120 kV and 114.1 mAs. The thickness of the CT scanned slices was 5mm, and the in-plane pixel size ranged from 0.579mm to 0.935mm. The number of chest CT scans for each patient ranged from 52 to 70. CT scans were performed using a Siemens Somatom Sensation 64 CT scanner in cohort 2. Image acquisition parameters consisted of 120 kV and 94 mAs. The thickness of the CT scanned slices was 1mm, and the in-plane pixel size ranged from 0.669mm to 0.815mm. The number of chest CT scans for each patient ranged from 300 to 370.

Due to the difference in CT data acquisition imaging between the two cohorts, the segmentation method was used to train the model in the two cohorts.

Automatic extraction of EAT

The proposed EAT segmentation is divided into four main modules, as shown in Supplementary Figure 1. By introducing the object detection module to improve the subsequent segmentation accuracy, the result of object detection is used to perform binary segmentation of the heart (myocardium and visceral pericardium) and background in the segmentation network to obtain the heart contour. The EAT is obtained by threshold extraction within the heart contour. Since there are many noise points in the result of threshold extraction, the development of threshold extraction is smoothed by post-processing.

The Yolo-V5[21] network was used for object detection, and the images containing the heart were used as the training samples to train the object detection model. The heart contour segmentation model is a classic U-Net network[22]. More details on the object detection network and segmentation network are provided in the Supplementary Methods.

As used in the generation of the reference, the threshold for adipose tissue has been defined as a Hounsfield Unit (HU) of -190HU to -30HU. EAT was obtained by threshold extraction and median filtering in the heart contour results obtained from the segmentation network.

In addition, a comparative test was carried out with a three-dimensional V-Net[23] network to explore whether object detection combined with a two-dimensional network is more conducive to segmentation.

CT radiomics features extraction and statistical analysis

Each patient's lung and EAT regions were formed into three-dimensional images, and 120 radiomics features[24] of both lung and EAT were extracted, respectively.

In a derivation cohort of 290 patients with COVID-19, univariate analysis and Pearson correlation analysis were used to identify predictors of COVID-19 severity classification from 120 lung and 120 EAT radiomics features. This analysis process refers to the method of Zhao et al [20]. Univariate logistic regression analysis was used to select features with significant differences. Then Pearson correlation analysis between features was conducted to exclude features with strong correlation. Finally, a generalized linear regression model was built in the derivation cohort (n=290), and then the improvement of the performance of the COVID-19 severity classification model by radiomics features of both lung and EAT was verified in the internal validation cohort (n=125) and the external validation cohort (n=100).

Precision and recall were used to evaluate the accuracy of the object detection model. DSC and Hausdorff distance (HD) were used to assess the validity of the segmentation model. The ROC curve analysis was used to calculate the AUC and select a cut-off value of severity classification, and calculate the accuracy (ACC), sensitivity (SN), and specificity (SP) of detecting severity. The estimated 95% Confidence Interval (CI) was calculated using 1000 bootstrap estimates. The improvement degree of the prediction effect of the model was evaluated according to the NRI and IDI. A more detailed description of each evaluation matrix is provided in the Supplementary Methods. Feature extraction, analysis, modeling, and evaluation were performed using Python (Version 3.7) and Pyradiomics (Version 3.0.1).

Results

Patient characteristics

In the derivation cohort, 30 (10.34%) patients were diagnosed with severe COVID-19. The mean age of mild and severe cases was 39.98 ± 15.39 and 59.23 ± 14.86 , respectively, and 48% (n=260) and 53% (n=30) were male, respectively. The baseline characteristics of patients in the derivation cohort are displayed in Table 1. There were no significant differences ($p > 0.05$) in gender, white blood cell count, potassium, and lactic acid.

In the internal validation cohort, 14 (11.2%) patients were diagnosed with severe COVID-19. The mean age of mild and severe cases was 40.46 ± 15.23 and 59.71 ± 14.46 , respectively, and 59% (n=111) and 79% (n=14) were male, respectively (Table 1). There were no significant differences ($p > 0.05$) in gender, white blood cell count, lactic acid, and creatinine.

Fifty patients (50%) were diagnosed with severe COVID-19 in the external validation cohort. The mean age of mild and severe cases was 46.22 ± 7.38 and 62.38 ± 16.14 , respectively, and 56% (n=28) and 60% (n=30) were male, respectively. There were no significant differences ($p > 0.05$) in gender.

EAT extraction

The DSC and HD distances in the test sets of the two cohorts are shown in table 1. The segmentation method using Yolo-V5+U-Net is significantly better than the other methods, with a DSC value of 0.972, while the HD is reduced by nearly half. The

prediction results of the U-Net network for all images are predicted as the background, the model is not optimized, and the DSC converges to 0.629. The prediction results are all blank negative samples, and HD cannot be calculated. In the test set, the visualization results of EAT segmentation results annotated by experts, and the results predicted by the model are compared, as shown in Figure 3. Detailed results of visualization of heart object detection and segmentation during EAT extraction are provided in Supplementary Results.

Feature selection and diagnostic model

One hundred and twenty radiomics features were extracted from lung and EAT, respectively. Feature selection is performed in the derivation cohort. Seventy-five lung and forty-two EAT radiomics features were significantly different in severity classification. The order of feature selection was ranked from high to low according to the AUC score of the univariate analysis. The feature importance scores are shown in Figure 4. The features with strong correlation were eliminated by correlation analysis among features (the correlation coefficient threshold was 0.75 in this paper). Finally, the remaining six lung radiomics features and four EAT radiomics features were included to build the diagnostic model (Table 2).

Based on six lung radiomics features, a basic diagnosis model was built. The AUC of the model in the derivation cohort was 0.87 (95%CI, 0.85-0.88). Radiomics features of both six lung and four EAT were used to compose the diagnostic model. After fitting, the AUC of the model in the derivation cohort was 0.95 (95% CI, 0.94-

0.96) (Table 3).

Model performance in the validation cohort

In the internal validation cohort, evaluating the model with lung radiomics features on this cohort yielded an AUC of 0.84 (95% CI, 0.81-0.87). At the optimal cut-off, the score had a SN of 64% (95%CI, 62%-66%), SP of 80% (95%CI, 77%-80%), and ACC of 78% (95%CI, 75%-80%). The results showed that the AUC of the model with radiomics features of both lung and EAT was 0.93 (95%CI, 0.91-0.95) (Table 3). At the optimal cut-off point, the SN was 79% (95%CI, 76-82%), SP was 88% (95%CI, 86%-90%), and ACC was 87% (95%CI, 86%-88%). Compared with the model with only lung features, the model with lung and EAT radiomics features demonstrated better predictive efficacy; its NRI increased by 22.4% ($p<0.001$), and IDI increased by 17% ($p<0.001$). ROC curves for different features combinations of the internal validation cohort are shown in Figure 5.a.

In the external validation cohort, an assessment of the model with the inclusion of lung radiomics features yielded an AUC of 0.73 (95% CI, 0.70-0.75). At the optimal cut-off, the score had a SN of 67% (95%CI, 66%-68%), SP of 78% (95%CI, 76%-80%), and ACC of 72% (95%CI, 69%-75%). The results showed that the external validation cohort's AUC score for the model with radiomics features of both lung and EAT was 0.77 (95%CI, 0.76 to 0.78). The SN was 73% (95%CI, 70%-76%), SP was 80% (95%CI, 76%-83%), and ACC was 77% (95%CI, 75%-79%) at the optimal cut-off point (Table 3). Compared with the model with only lung features, the model with radiomics features

of both lung and EAT demonstrated better predictive performance; its NRI increased by 11.1% ($p < 0.001$), and IDI increased by 8% ($p < 0.001$). ROC curves for different features combinations of the external validation cohort are shown in Figure 5.b.

In addition, the inclusion of clinical variables in the model found that adding radiomics features of both EAT and lung based on the clinical variable model can also improve the SN, SP, AUC, and ACC, as shown in the Supplementary Results.

Discussion

This paper investigates a fully automated EAT extraction method and the value of EAT radiomics features for severity stratification in COVID-19 patients. Main findings:(1) a method is proposed to improve the accuracy of EAT extraction, and (2) the radiomics features of EAT combined with lung have incremental value in detecting the severity of COVID-19 infection.

The treatment of patients with mild and severe COVID-19 is different. Severe patients need more medicine to prevent their condition from worsening, and mild patients need to warn their doctors to optimize treatment plans when their symptoms become severe. Therefore, it is necessary to predict the severity of COVID-19 infection. At present, the diagnosis of mild and severe cases is mainly based on patients' clinical indicators and lung radiomics features. For example, in clinical symptoms, the oxygen saturation of severe patients in the resting state is less than 93% and respiratory distress occurs. In lung imaging, severe patients showed diffuse lung lesions with extensive exudation and consolidation of lung parenchyma. Zhang et al.[25] used machine learning to classify patients' blood indicators for mild and severe cases of COVID-19.

The naïve Bayes model was the best with an AUC of 0.90. Li et al.'s[26] AUC for light and severe classification of CT visual quantitative score of patients could reach 0.918. However, acquiring clinical indicators takes time, and the increase in diagnosis time may lead to missing the best treatment. Diagnostic methods that rely on imaging features only focusing on the lung region lack comprehensive judgment, because of COVID-19, especially in severe patients, may lead to complications in other parts of the patient's body. As confirmed in previous studies, the heart is one of the main complications [1, 27, 28]. Therefore, the detection of cardiac effects of COVID-19 should also be used as a factor for severity stratification, providing more possibilities for more accurate stratification of COVID-19. EAT was selected as a target for the impact of COVID-19 on the heart because the coronary artery and myocardium are closely adjacent to it, and it can secrete many anti-inflammatory and pro-inflammatory adipokines, which are closely associated with the occurrence of adverse cardiovascular events in many studies[7, 8, 12-14].

In a study by Wei et al.[12], the assessment of pre-hospital disease in combination with EAT volume obtained from chest CT scans found that EAT could provide a valuable threshold point for predicting COVID-19 cardiovascular complications. Kim et al.[14] analyzed the relationship between EAT and COVID-19 at the biological level. It can be concluded that EAT may be the main factor of SARS-CoV-2 entering the heart. Bihan et al.[15] found an association between EAT volume and the severity of COVID-19 infection, which helps to assess the risk of disease progression. However, in previous studies, the extraction method of EAT needs to be optimized, and EAT's analysis mainly

focuses on EAT volume analysis. With the development of Radiomics, more valuable radiomics features can be explored to support the research.

In the extraction of EAT, the proposed method is 0.079 higher than the DSC proposed by Hoori et al.[18] and 0.149 higher than the DSC proposed by Commandeur et al.[19]. The improvement of extraction effect of EAT is due to the influence of negative samples sent by the object detection module before segmentation, which improves the accuracy of segmentation. By testing, the operating time for the segmentation and extraction of EAT from a patient's chest CT data on a standard computer was less than 20 seconds, compared with about 20 minutes for manual extraction by a specialist. These can significantly reduce the waste of time, making it more convenient to extract EAT and carry out meaningful research.

As in previous studies, EAT was found to be related to the severity of COVID-19 in terms of severity stratification. In this study, it was found that combining radiomics features of both lung and EAT improved the performance of the diagnostic model. In the internal validation cohort, the NRI and IDI of the model with EAT radiomics features respectively increased by 22.4% and 17.0% compared with the model with only lung radiomics features. In the external validation cohort, the NRI and IDI increased by 11.1% and 8.0%, respectively. However, our analysis included more radiomic features of EAT and found other meaningful features which were not found in previous studies. The ZoneEntropy and Skewness of EAT were identified as essential radiomics features. These two features reflect the uncertainty or randomness of the size and gray distribution of the measurement area and the asymmetry of the value

distribution on the mean value, respectively. The adipose tissue attenuation value is a dynamic interval [-190, -30], so these two features show the instability of adipose tissue attenuation value in the EAT region of the image. In previous studies[29], cardiovascular risk was assessed by the fat attenuation index. This study showed that adipose tissue could influence inflammation by releasing bioactive adipokines, thus influencing the fat attenuation index. Considering that EAT is a pro-inflammatory medium, we hypothesized that COVID-19 would affect EAT in severe patients and lead to increased adipose tissue activity. These may explain the uncertainty of gray distribution and the asymmetry of value distribution in the EAT radiomics features.

Our study still has a few limitations. Firstly, in the segmentation model, two segmentation models need to be trained to complete the segmentation of the heart contour due to the imaging difference between the two centers' data. Secondly, less severe data in cohort 1 may lead to data imbalance, and more balanced data should be included in further study.

Acknowledgments

This research was supported by the Henan Science and Technology Development Plan 2022 (Project Number: 222102210219) and the National Outstanding Youth Science Fund Project of National Natural Science Foundation of China under Grant 62106233.

References

- 1 Long B, Brady WJ, Koefman A, Gottlieb M (2020) Cardiovascular complications in COVID-19. *Am J Emerg Med* 38:1504-1507
- 2 World Health O (2020) Coronavirus disease (COVID-19): situation report, 190. World Health Organization, Geneva
- 3 Xie Z, Sun H, Wang J et al (2021) A novel CT-based radiomics in the distinction of severity of coronavirus disease 2019 (COVID-19) pneumonia. *BMC Infectious Diseases* 21:608
- 4 Qiu J, Peng S, Yin J et al (2021) A Radiomics Signature to Quantitatively Analyze COVID-19-Infected Pulmonary Lesions. *Interdisciplinary Sciences: Computational Life Sciences* 13:61-72
- 5 Zhu F, Zhu Z, Zhang Y et al (2022) Severity detection of COVID-19 infection with machine learning of clinical records and CT images. *Technology and Health Care Preprint*:1-16
- 6 Gong J, Dong H, Xia Q-S et al (2020) Correlation analysis between disease severity and inflammation-related parameters in patients with COVID-19: a retrospective study. *BMC Infectious Diseases* 20:963
- 7 Matloch Z, Kotulak T, Haluzik M (2016) The role of epicardial adipose tissue in heart disease. *Physiol Res* 65:23-32
- 8 Nalliah CJ, Bell JR, Raaijmakers AJA et al (2020) Epicardial Adipose Tissue Accumulation Confers Atrial Conduction Abnormality. *J Am Coll Cardiol* 76:1197-1211
- 9 Feng X, Li S, Sun Q et al (2020) Immune-Inflammatory Parameters in COVID-19 Cases: A Systematic Review and Meta-Analysis. *Frontiers in Medicine* 7
- 10 Wei JF, Huang FY, Xiong TY et al (2020) Acute myocardial injury is common in patients with COVID-19 and impairs their prognosis. *Heart* 106:1154-1159
- 11 Huang C, Wang Y, Li X et al (2020) Clinical features of patients infected with 2019 novel coronavirus in Wuhan, China. *The Lancet* 395:497-506
- 12 Wei ZY, Qiao R, Chen J et al (2020) Pre-existing Health Conditions and Epicardial Adipose Tissue Volume: Potential Risk Factors for Myocardial Injury in COVID-19 Patients. *Front Cardiovasc Med* 7:585220
- 13 Wang D, Hu B, Hu C et al (2020) Clinical Characteristics of 138 Hospitalized Patients With 2019 Novel Coronavirus-Infected Pneumonia in Wuhan, China. *JAMA* 323:1061-1069
- 14 Kim IC, Han S (2020) Epicardial adipose tissue: fuel for COVID-19-induced cardiac injury? *Eur Heart J* 41:2334-2335
- 15 Bihan H, Heidar R, Beloeuvre A et al (2021) Epicardial adipose tissue and severe Coronavirus Disease 19. *Cardiovasc Diabetol* 20:147
- 16 Ilyushenkova J, Shelemekhov A, Popov E, Sazonova S, Batalov R, Popov S (2021) Potential role of CT-radiomics of epicardial adipose tissue in the prognosis of atrial fibrillation catheter ablation outcome. *European Heart Journal - Cardiovascular Imaging* 22
- 17 Yang M, Cao Q, Xu Z et al (2022) Development and Validation of a Machine Learning-Based Radiomics Model on Cardiac Computed Tomography of Epicardial Adipose Tissue in Predicting Characteristics and Recurrence of Atrial Fibrillation. *Frontiers in Cardiovascular Medicine* 9
- 18 Hoori A, Hu T, Al-Kindi S, Rajagopalan S, Wilson DL (2021) Automatic Deep Learning Segmentation and Quantification of Epicardial Adipose Tissue in Non-Contrast Cardiac CT scans. *Annu Int Conf IEEE Eng Med Biol Soc* 2021:3938-3942
- 19 Commandeur F, Goeller M, Betancur J et al (2018) Deep Learning for Quantification of Epicardial and Thoracic Adipose Tissue From Non-Contrast CT. *IEEE Trans Med Imaging* 37:1835-1846

- 20 Zhao C, Xu Y, He Z et al (2021) Lung segmentation and automatic detection of COVID-19 using radiomic features from chest CT images. *Pattern Recognit* 119:108071
- 21 Glenn Jocher AS, Jirka Borovec, NanoCode012 et al (Apr.2021.) ultralytics/yolov5: v5.0-YOLOv5-P6 1280 models, AWS, Supervise.ly and YouTube integrations,
- 22 Ronneberger O, Fischer P, Brox T (2015) U-Net: Convolutional Networks for Biomedical Image Segmentation. In: Navab N, Hornegger J, Wells WM, Frangi AF, (eds) *Medical Image Computing and Computer-Assisted Intervention – MICCAI 2015*. Springer International Publishing, Cham, pp 234-241
- 23 Milletari F, Navab N, Ahmadi S (2016) V-Net: Fully Convolutional Neural Networks for Volumetric Medical Image Segmentation 2016 Fourth International Conference on 3D Vision (3DV), pp 565-571
- 24 Zwanenburg A, Vallieres M, Abdalah MA et al (2020) The Image Biomarker Standardization Initiative: Standardized Quantitative Radiomics for High-Throughput Image-based Phenotyping. *Radiology* 295:328-338
- 25 Zhang RK, Xiao Q, Zhu SL, Lin HY, Tang M (2022) Using different machine learning models to classify patients into mild and severe cases of COVID-19 based on multivariate blood testing. *JOURNAL OF MEDICAL VIROLOGY* 94:357-365
- 26 Li KW, Fang YJ, Li WJ et al (2020) CT image visual quantitative evaluation and clinical classification of coronavirus disease (COVID-19). *European Radiology* 30:4407-4416
- 27 Krittanawong C, Kumar A, Hahn J et al (2020) Cardiovascular risk and complications associated with COVID-19. *American Journal of Cardiovascular Disease* 10:479-489
- 28 Linschoten M, Peters S, van Smeden M et al (2020) Cardiac complications in patients hospitalised with COVID-19. *European Heart Journal-Acute Cardiovascular Care* 9:817-823
- 29 Kluner LV, Oikonomou EK, Antoniades C (2021) Assessing Cardiovascular Risk by Using the Fat Attenuation Index in Coronary CT Angiography. *Radiol Cardiothorac Imaging* 3:e200563

Figure legends

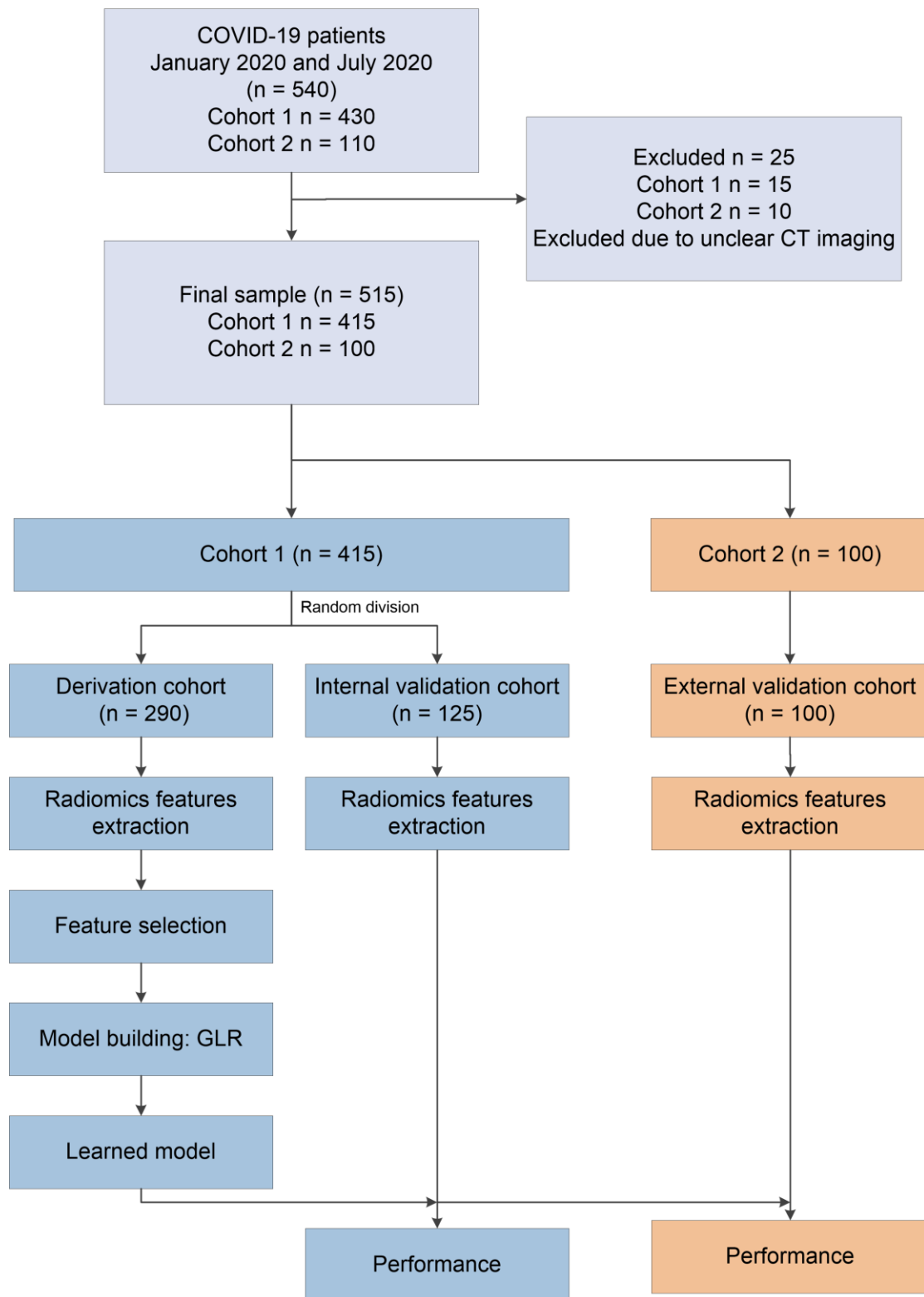


Figure 1 Flowchart of patient inclusion and exclusion and flowchart for Derivation, Internal Validation, and External Validation.

GLR, generalized linear regression.

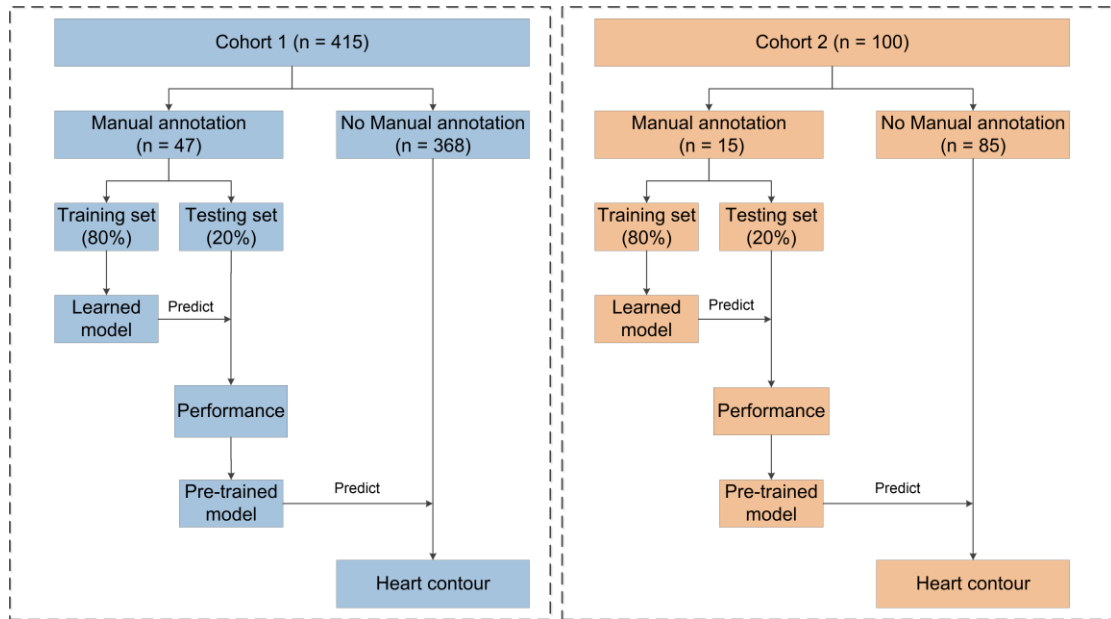


Figure 2 Flowchart of heart contour segmentation data processing.

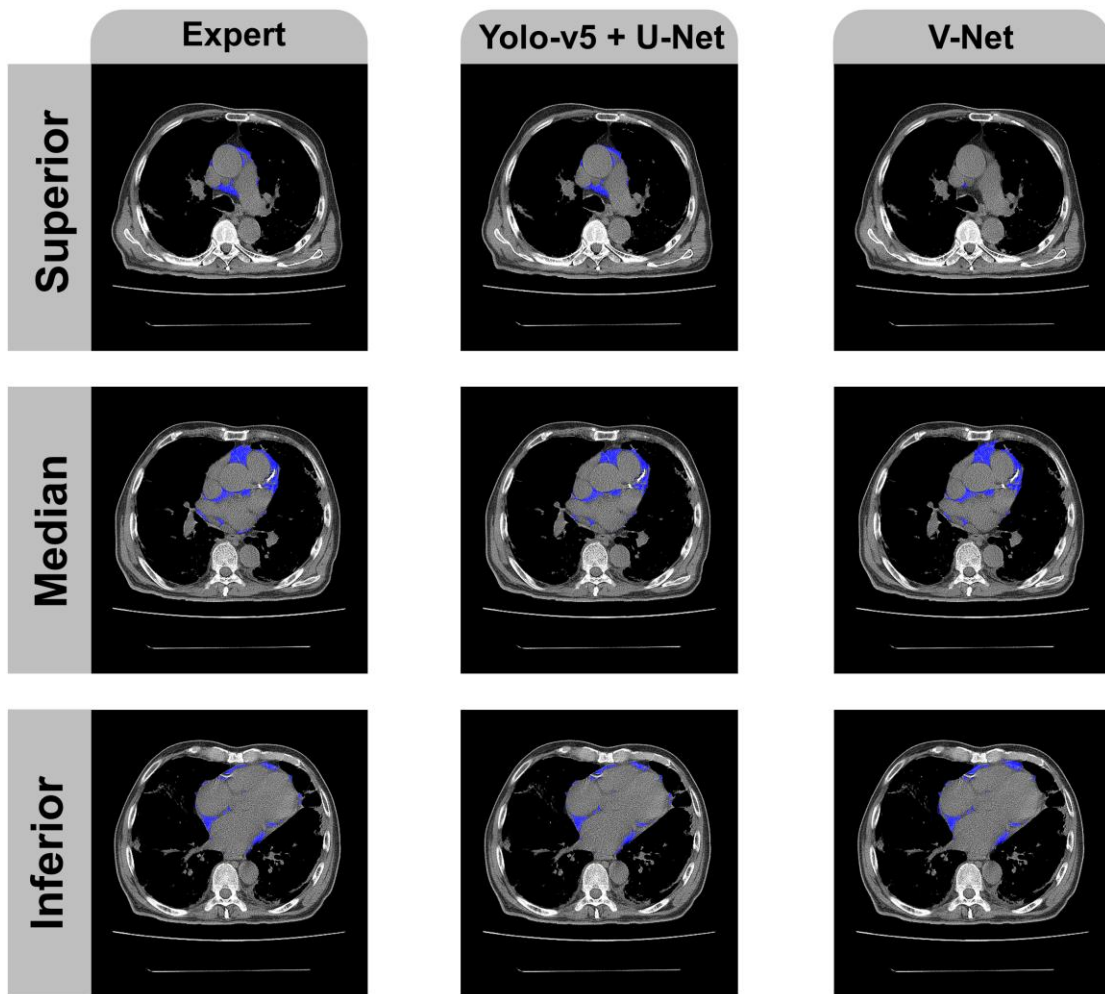


Figure 3 Comparison of the results of EAT extraction.

Comparison of the results of EAT extraction based on expert segmentation (left column), automatic heart segmentation by Yolo-V5+U-Net method (middle column, DSC=0.972), and automatic heart segmentation by V-Net method (right column, DSC=0.921) in cohort 1. The blue area is EAT. The upper, middle, and lower rows correspond to the upper, middle, and lower parts of the heart.

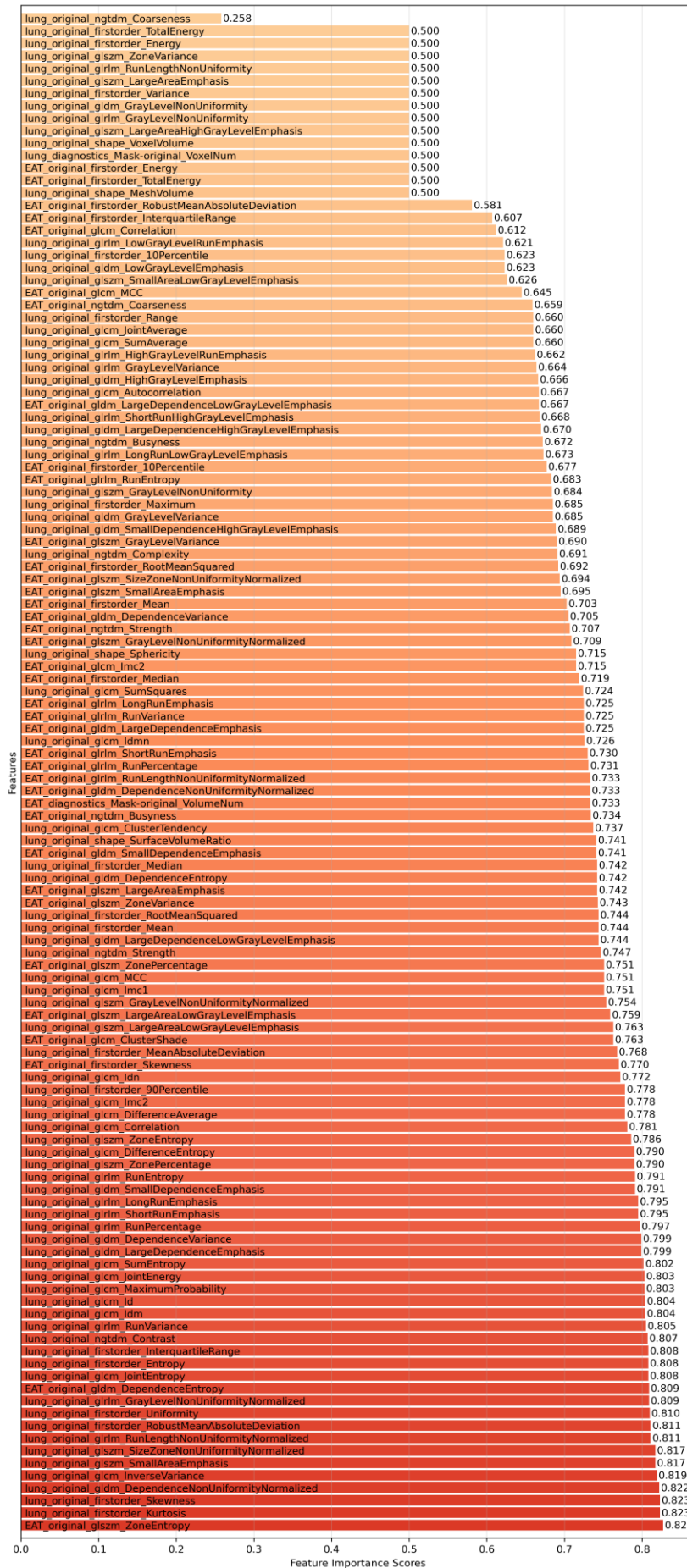


Figure 4 Feature importance scores.

The left side of the bar shows the name of each feature, and the right side of the bar shows the feature importance score of the corresponding feature.

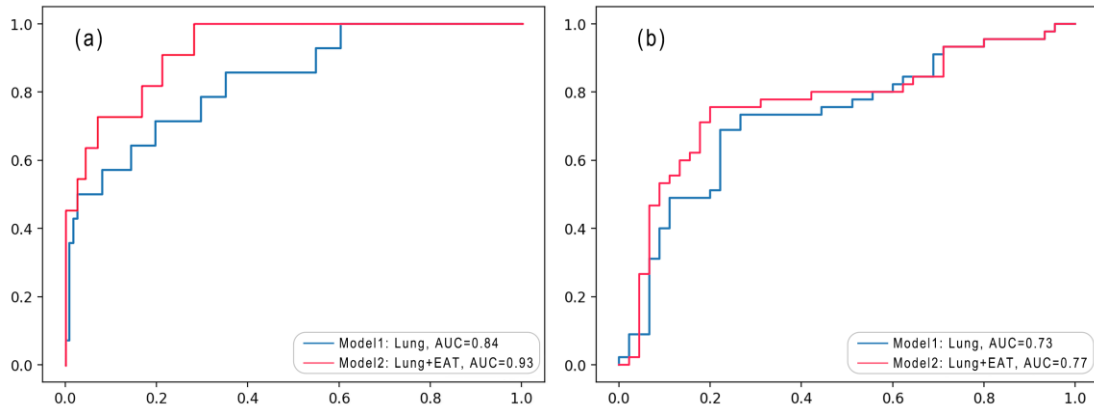


Figure 5 (a) Receiver operating characteristic curves for different features combinations of the internal validation cohort (n=125). (b) Receiver operating characteristic curves for different features combinations of the external validation cohort (n=90).

The blue line is the model with only lung radiomics features, and the red line is the model with radiomics features of both lung and EAT.

AUC, area under the receiver operating characteristic curve.

Tables legends

Table 1 Baseline Characteristics of Patients in the Derivation and Internal Validation Cohort Mild and Severe COVID-19.

Characteristics	Derivation Cohort		P	Internal Validation Cohort		P
	Mild	Severe		Mild	Severe	
Age, years, mean(±SD)	39.98±15.39	59.23±14.86	<.001	40.46±15.23	59.71±14.46	<.001
Gender, No. (%)			.59			.15
Male	125(48)	16(53)		65(59)	11(79)	
Female	135(52)	14(47)		46(41)	3(21)	
Past cardiovascular disease, No. (%)	35(13)	13(43)	<.001	16(14)	5(36)	.045
Lactate dehydrogenase, (U/L), mean(±SD)	219.37±61.10	346.47±142.47	<.001	220.29±83.26	326.29±102.63	<.001
NTPro-BNP, (pg/ml), mean(±SD)	4.22±0.94	4.19±1.01	.84	4.26±0.83	3.71±0.62	.02
Creatine kinase isoenzymes, (ng/ml), mean(±SD)	13.19±12.07	16.43±10.69	.16	12.61±4.66	12.91±2.37	.82
Hypertension, No. (%)	31(12)	9(30)	.01	16(14)	5(36)	.045
D-dimer, (ug/ml), mean(±SD)	0.55±1.34	1.72±3.70	<.001	0.57±1.64	2.23±4.96	.01
White blood cell, (10 ⁹ /L), mean(±SD)	5.55±1.90	5.37±1.94	.61	5.38±2.39	6.22±4.61	.29
Lymphocyte, (10 ⁹ /L), mean(±SD)	1.44±0.60	1.02±0.41	<.001	1.45±0.49	0.93±0.61	<.001
Serum sodium, (mmol/L), mean(±SD)	139.90±2.70	137.70±3.77	<.001	139.98±2.04	134.29±5.20	<.001
Urea, (mmol/L), mean(±SD)	4.43±1.50	5.56±3.46	<.001	4.43±1.13	5.04±2.09	.09
PO ₂ , (KPa), mean(±SD)	14.34±4.34	9.94±4.94	<.001	14.68±4.75	13.45±5.51	.38
PCO ₂ , (KPa), mean(±SD)	5.43±0.45	5.49±0.89	.66	5.39±0.59	4.94±0.72	.01
PCT, (ng/ml), mean(±SD)	0.04±0.03	0.18±0.39	<.001	0.04±0.04	0.16±0.18	<.001
APTT, (s), mean(±SD)	38.57±6.35	42.06±6.57	.01	38.02±4.10	43.10±5.69	<.001
PT, (s), mean(±SD)	13.38±1.10	13.62±0.83	.26	13.29±0.60	13.73±1.46	.04
Potassium, (mmol/L), mean(±SD)	3.80±0.34	3.79±0.36	.89	3.83±0.34	3.58±0.43	.02
Lactic acid, (mmol/L), mean(±SD)	1.26±1.20	1.37±1.03	.62	1.29±0.81	0.94±0.22	.11
HDL-C, (mmol/L), mean(±SD)	29.23±3.90	28.46±3.77	.31	29.02±3.80	26.26±3.14	.01
eGFR, (ml/(min*1.73m ²)), mean(±SD)	117.13±25.09	106.31±29.54	.03	118.49±22.74	108.55±29.74	.14
Creatinine, (umol/L), mean(±SD)	65.30±19.22	69.14±33.25	.35	64.35±14.09	70.31±21.95	.17
LDL-C, (mmol/L), mean(±SD)	24.46±1.84	24.51±2.49	.89	24.37±1.77	24.56±2.44	.73
ALT, (U/L), mean(±SD)	25.03±18.11	29.23±19.50	.24	29.72±22.25	36.08±35.10	.36
AST, (U/L), mean(±SD)	24.61±19.05	37.50±25.24	<.001	24.56±12.24	37.51±23.90	<.001
Dyspnea, No. (%)	6(2)	2(7)	.18	2(2)	5(36)	<.001
Diabetes, No. (%)	14(5)	3(10)	.31	4(4)	3(21)	.01
Antivirals, No. (%)	161(56)	29(97)	<.001	73(66)	13(93)	.04
Exudative lesions, No. (%)	50(17)	10(33)	.07	16(14)	2(14)	.99
CAD, No. (%)	5(2)	4(13)	<.001	0(0)	0(0)	-

ALT, alanine aminotransferase; APTT, activated partial thrombin time; AST, aspartate aminotransferase; CAD, coronary heart disease; eGFR, estimated glomerular filtration rate; HDL-C, high density liprotein cholesterol; LDL-C, low density lipoprotein cholesterol; PCO₂, partial pressure of carbon dioxide; PCT, procalcitonin; PO₂, partial pressure of oxygen; NTPRO-BNP, NT pro B-type natriuretic peptide; PT, prothrombin time.

Table 2 Comparison of different DSC and HD methods in two cohort test sets.

	Model	DSC	HD(mm)
Cohort 1	U-Net	0.629(\pm 0.047)	-
	V-Net	0.921(\pm 0.019)	14.446(\pm 3.143)
	Yolo-V5 + U-Net	0.972(\pm0.011)	7.538(\pm2.112)
Cohort 2	U-Net	0.653(\pm 0.032)	-
	V-Net	0.903(\pm 0.024)	17.169(\pm 5.168)
	Yolo-V5 + U-Net	0.968(\pm0.005)	6.423(\pm1.842)

DSC, Dice similarity coefficient; HD, Hausdorff distance.

Table 3 Features used in diagnostic models. Features were ranked according to the AUC in univariate analysis.

Features of the source	Features
EAT	original_glszm_ZoneEntropy
Lung	original_firstorder_Kurtosis
Lung	original_glszm_SmallAreaEmphasis
EAT	original_firstorder_Skewness
Lung	original_glszm_LargeAreaLowGrayLevelEmphasis
EAT	original_glszm_LargeAreaLowGrayLevelEmphasis
Lung	original_glcmm_MaximalCorrelationCoefficient
EAT	original_glszm_ZonePercentage
Lung	original_ngtdm_Strength
Lung	original_ngtdm_Complexity

Table 4 Model Fitting and Calibration in the Derivation Cohort (n = 290) and the predictive performance of the internal validation cohort (n=125) and external validation cohort (n=90) for the mild and severe classification.

Cohort	Features	SN	SP	AUC	ACC	P
Derivation	Lung	0.80	0.84	0.87	0.83	<.001
	Lung+EAT	0.90	0.84	0.95	0.85	<.001
Internal Validation	Lung	0.64	0.80	0.84	0.78	<.001
	Lung+EAT	0.73	0.88	0.93	0.86	<.001
External Validation	Lung	0.67	0.78	0.73	0.72	<.001
	Lung+EAT	0.73	0.80	0.77	0.77	<.001

ACC, accuracy; AUC, area under the receiver operating characteristic curve; SN, sensitivity; SP, specificity.

